Theoretical investigation on the effect of volume fraction in the optical trapping of gold nanoparticles

Zhu, Zheng; Zhang, Yu Quan; Adam, Aurèle J.L.; Min, Changjun; Urbach, H. Paul; Yuan, Xiaocong

DOI
10.1016/j.optcom.2023.129572

Publication date
2023

Document Version
Final published version

Published in
Optics Communications

Optics Communications 541 (2023) 129572

Contents lists available at ScienceDirect

Optics Communications

journal homepage: www.elsevier.com/locate/optcom

Theoretical investigation on the effect of volume fraction in the optical trapping of gold nanoparticles

Zheng Zhu [a,b], YuQuan Zhang [a,*], Aurèle J.L. Adam [b,*], Changjun Min [a], H.Paul. Urbach [b], Xiaocong Yuan [a]

[a] Nanophotonics Research Center, Shenzhen Key Laboratory of Micro-Scale Optical Information Technology & Institute of Microscale Optoelectronics, Shenzhen University, 518060, Shenzhen, China

[b] Optics Research Group, Delft University of Technology, Lorentzweg 1, 2628 CJ, Delft, The Netherlands

ARTICLE INFO

Keywords:
Optical tweezer
Optical force
Optical potential well
Gold nanoparticle

ABSTRACT

Stable optical trapping of gold nanoparticles is essential and desirable because of its wide applications in nanotechnology. While several factors have been proposed to affect optical trapping stability, the sample's volume fraction during optical trapping has often been neglected. To address this, by utilizing the effective medium theory, we analyze the stability of optical trapping of a gold nanoparticle in human serum albumin solutions, HIV-1,virus solutions, and gold nanoparticle solutions in this article. Our comparative analysis of the optical force and potential on a single gold nanoparticle in solutions of varying volume fractions reveals that both parameters decrease with increasing volume fraction. This finding can aid in more effective control of gold nanoparticles in various applications.

1. Introduction

Optical tweezer has yielded many interesting applications over the past few decades since Ashkin developed the first laser trapping and captured micrometer-size particles [1]. For example, it can be used as a highly sensitive force transducer [2–4] to monitor forces in the pico-Newton regime and to measure distances in the nanometer range. Metallic nanoparticles, especially gold nanoparticles, are efficient and natural probes. Compared to other probes, such as quantum dots and organic dyes, gold nanoparticles can be biologically harmless when exposed to light for prolonged periods [5]. In addition, the optical forces exerted on gold nanoparticles are several times greater than those exerted on dielectric nanoparticles [6]. Gold nanoparticles have been widely used in biomedical experiments, for instance, in the diagnosis of cancer cells [7], the detection of DNA [8,9], delivery of therapeutic drugs [10], and monitoring the motion of protein [11]. Therefore, it is important to analyze optical forces and potentials for the stable optical trapping of a single gold nanoparticle in a wide range of applications.

Optical trapping of gold nanoparticles in liquid has made significant progress since its first report in 1994 [6], including the extension of nanoparticle size to diameters between 5 and 250 nm [12], and even controlling the orientation of nanorods [13,14]. However, due to the strong scattering force and the unavoidable Brownian motion in the water, it is challenging to achieve stable optical trapping of gold nanoparticles with a radius ranging between 1 and 50 nm [15]. Quantitative analysis of the optical force is crucial for optimizing the stability of optical trapping. Stable optical trapping is the consequence of the interplay of different factors. The optical forces depend highly on the size of the particle. When the particle size is smaller than, or on the order of the skin depth of the gold, the gradient force is proportional to the polarized volume of the particle on the basis of experiment results [16]. When the radius is significantly larger than the skin depth of the gold for a given wavelength, the gradient force increases slowly because of the attenuation of the incident field in the particle. An increase in the size of the nanoparticle also leads to a larger extinction cross-section, which results in an enlargement of the scattering force. Besides the factors mentioned above, for the sample in the liquid environment, the effect of its volume fraction on the optical trapping of a gold nanoparticle has not yet been investigated.

In practical biological experiments, the presence of aqueous solutions with high bio-sample concentrations is inevitable [17,18]. This study highlights the critical role of the volume fraction of the sample in the stability of optical trapping of a gold nanoparticle in various solutions, including gold nanoparticle solutions, human serum albumin solutions, and HIV-1 virus solutions. The effective refractive index of the composite material is analyzed for three different sample solutions. The focused optical field can be expressed analytically using the theory of vectorial diffraction. [19]. By achieving comparative studies of the optical force and potential on a single gold nanoparticle with three different volume fractions in each solution, we demonstrate that stable

* Corresponding authors.
E-mail addresses: yqzhang@szu.edu.cn (Y. Zhang), A.J.L.Adam@tudelft.nl (A.J.L. Adam).

https://doi.org/10.1016/j.optcom.2023.129572
Received 7 February 2023; Received in revised form 6 April 2023; Accepted 3 May 2023
Available online 9 May 2023

optical trapping depends on the volume fraction of the sample. Our calculations show that the optical force on the trapped gold nanoparticle weakens, and the depth of the potential well reduces as the volume fraction of the corresponding sample increases. These results provide valuable insights for optimizing the stability of optical trapping in various applications.

2. Theory

The time-average optical forces on a particle (radius $\ll \lambda$) are usually described as the sum of two terms [20]:

$$\langle \mathbf{F} \rangle_{\text{total}} = \langle \mathbf{F} \rangle_{\text{grad}} + \langle \mathbf{F} \rangle_{\text{scatter}}, \tag{1}$$

$$\langle \mathbf{F} \rangle_{\text{grad}} = \frac{1}{4}\text{Re}\{\alpha\}\nabla|\mathbf{E}|^2, \tag{2}$$

$$\langle \mathbf{F} \rangle_{\text{scatter}} = \frac{1}{2}\sigma\text{Re}\left\{\frac{1}{c}\mathbf{E}\times\mathbf{H}^*\right\}, \tag{3}$$

where α is the scalar polarizability of the gold nanoparticle, ε_0 is the permittivity of the vacuum, c is the speed of light in vacuum, $\mathbf{E}$ and $\mathbf{H}$ are the electric field and magnetic field. ε_0 is the permittivity of the vacuum. k ($k = 2\pi\mathbf{n}_{\text{eff}}/\lambda$) is the wave number of the incident optical field in the liquid containing the nanoparticles. $\mathbf{n}_{\text{eff}}$ is the complex refractive index of the mixture material. The first term of Eq. (1) is the gradient force that is originally from the inhomogeneous electric energy density. The absorbing and scattering forces are written in the approximation of small spheres through the absorbing and scattering cross sections [21]. In this paper, following the traditional convention, the second term is defined as the scattering force. Especially for metallic nanoparticles, the absorption of light by the particle can significantly contribute to the scattering force [22,23]. The total cross section is the sum of the scattering cross section σ_{sca} and absorptive cross section σ_{abs} ($\sigma = \sigma_{sca} + \sigma_{abs} = k\text{Im}\{\alpha\}/\varepsilon_0$) [20]. In addition, the spin curl force arises from the spin angular momentum, but this can be neglected for optical fields with linear polarization [20]. The whole optical trapping process can be seen as a gold nanoparticle being trapped in a composite medium with an external electromagnetic field focused on it.

In the Rayleigh regime ($r < \lambda/20$), a small particle can be modeled as an electric dipole in response to the incident optical field. For a gold nanoparticle with relative permittivity ε_p embedded in a host medium with relative permittivity ε_h, the scalar polarizability α_0 can be deduced using the conservation law of momentum at the boundary between the metallic particle and the host medium [24]. After adding the radiative reaction correction [25], an accurate formula for the polarizability α for a dipole can be derived as [26,27]

$$\alpha_0 = 4\pi\varepsilon_0 r^3 \frac{\varepsilon_p - \varepsilon_h}{\varepsilon_p + 2\varepsilon_h}, \tag{4}$$

$$\alpha = \alpha_0\left(1 + \frac{2i}{3}\frac{\varepsilon_p - \varepsilon_h}{\varepsilon_p + 2\varepsilon_h}(kr)^3\right). \tag{5}$$

The gradient force and the scattering force are strongly size dependent. For gold nanoparticles with refractive index $\boldsymbol{n}_p = n_0 + i\kappa_0$, the depth of the skin of gold can be described as $\sigma = \lambda/2\pi\kappa_0$[28]. When a large particle cannot be approximated as a dipole, the optical force on a particle can be calculated with a rigorous electromagnetic model such as the Maxwell stress tensor (MST) method [29].

The magnitude of the minimal potential determines the stiffness and efficiency of optical trapping. The trapping potential is normalized to k_BT, which is usually used to describe the energy of Brownian motion of the particle in the aqueous environment. A requirement for stable optical trapping is that the depth of the potential well is deeper than 10 k_BT [30]. Here, k_B is Boltzmann constant and T is the absolute temperature of the environment, which is chosen to be equal to 300 K. Three orthogonal paths $\boldsymbol{r}$ were chosen to obtain the potential $U(\mathbf{r})$ using the expression below.

$$U(\mathbf{r}) = -\int_{\infty}^{r} \langle \mathbf{F}(\mathbf{r}) \rangle_{\text{total}}\, d\mathbf{r}. \tag{6}$$

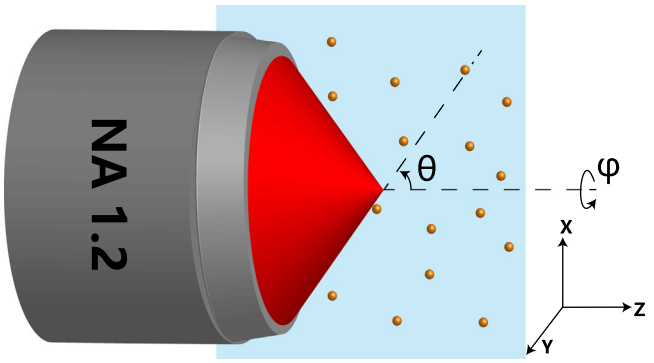

Fig. 1. Schematic picture of the calculation. An x-polarized Gaussian beam propagates through a high NA objective. A gold nanosphere with a 15 nm radius is trapped in the focused optical field. The NA of the objective is 1.2 and the average power is 500 mW. Three kinds of composite medium (the human serum albumin solution, the HIV-1 solution, and the gold nanoparticle solution) are used in the simulation.

For the dispersal of metal nanoparticles in liquid, the Maxwell–Garnett (MG) mixing rule can be used to describe the equivalent permittivity of a composite medium. The effective permittivity can be written as [31]

$$\varepsilon_{\text{eff}} = \varepsilon_h\left[1 + 3f\Gamma\left(1 + i\frac{2}{3}(kr)^3\Gamma\right)\right], \tag{7}$$

$$\Gamma = \frac{\chi}{1 - f\chi}, \quad \chi = \frac{(\varepsilon_p - \varepsilon_h)}{(\varepsilon_p + 2\varepsilon_h)}. \tag{8}$$

where ε_{eff} is the permittivity of the liquid containing the particle and f ($f = 4\pi Nr^3/3V$) is the volume fraction of the gold nanoparticle in the solution and N is the number of dipoles in a volume V. Eq. (7) is called the MG mixing rule. The radius of the gold particle is 15 nm in our simulation.

HIV-1 virus with 50 nm radius [32] is selected as the large biosample in our simulations. For the optically soft sample of large size in the solution, such as the virus or soft tissue, the interface scattering and absorption is negligible [33]. The simple mixing rule is often used in biology applications without considering the shape of the inclusions and the topology of the composite material [34]. The effective index of refraction can be obtained as a function of volume fraction f_1:

$$n_{\text{eff}} = n_p f_1 + (1 - f_1)n_h. \tag{9}$$

where n_{eff} is the effective refractive index of the composite material; n_p is the refractive index of the sample; n_h is the refractive index of the host medium. f_1 is the volume fraction of the sample in the solution.

For the composite medium consisting of small sample and liquid, such as protein solution or DNA solution, we introduce the extended Lorenz–Lorenz equation [35]:

$$\frac{n_{\text{eff}}^2 - 1}{n_{\text{eff}}^2 + 2} = f_2\frac{n_p^2 - 1}{n_p^2 + 2} + (1 - f_2)\frac{n_h^2 - 1}{n_h^2 + 2}, \tag{10}$$

f_2 is the volume fraction of the dipole in the solution. Human serum albumin with a radius of 2.74 nm [36] is used as a small sample in our simulation.

The configuration with the coordinate system is shown in Fig. 1. The host medium is water in our simulation. For a stable optical trapping of small gold nanoparticles, a high-intensity focused beam is necessary to provide a force large enough to counteract Brownian motion. An x-polarized Gaussian beam with an average power of 500 mW is used as incident light. The wavelength of incident light λ is set at 633 nm for the gold nanoparticle solution. The refractive index of the HIV-1 virus is 1.5 and λ = 633 nm [32]. The wavelength of incident light λ is 589 nm for the human serum albumin solution and the refractive index of human serum albumin is 1.603 [35]. The refractive index of the gold nanoparticle is 0.274+2.94i at 589 nm and 0.183+3.43i at 633 nm [37].

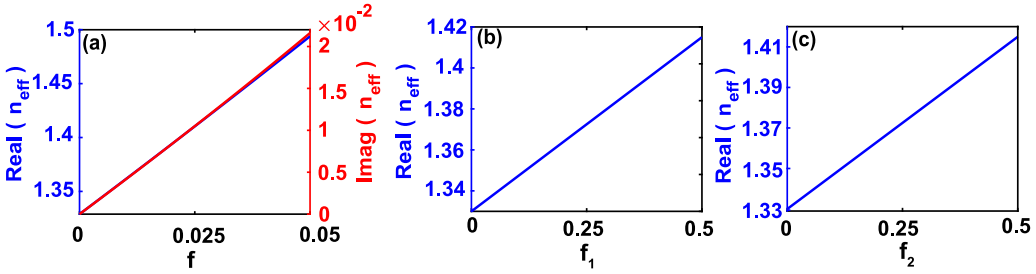

Fig. 2. Comparison in the effective refractive index of three composite mediums: (a) gold nanoparticle solution at $\lambda = 633$ nm, (b) Virus solution (HIV-1 virus) at $\lambda = 633$ nm, and (c) protein solution (human serum albumin) at $\lambda = 589$ nm. The real and imaginary parts of the refractive index are plotted by the blue line and red line. The surrounding environment is water.

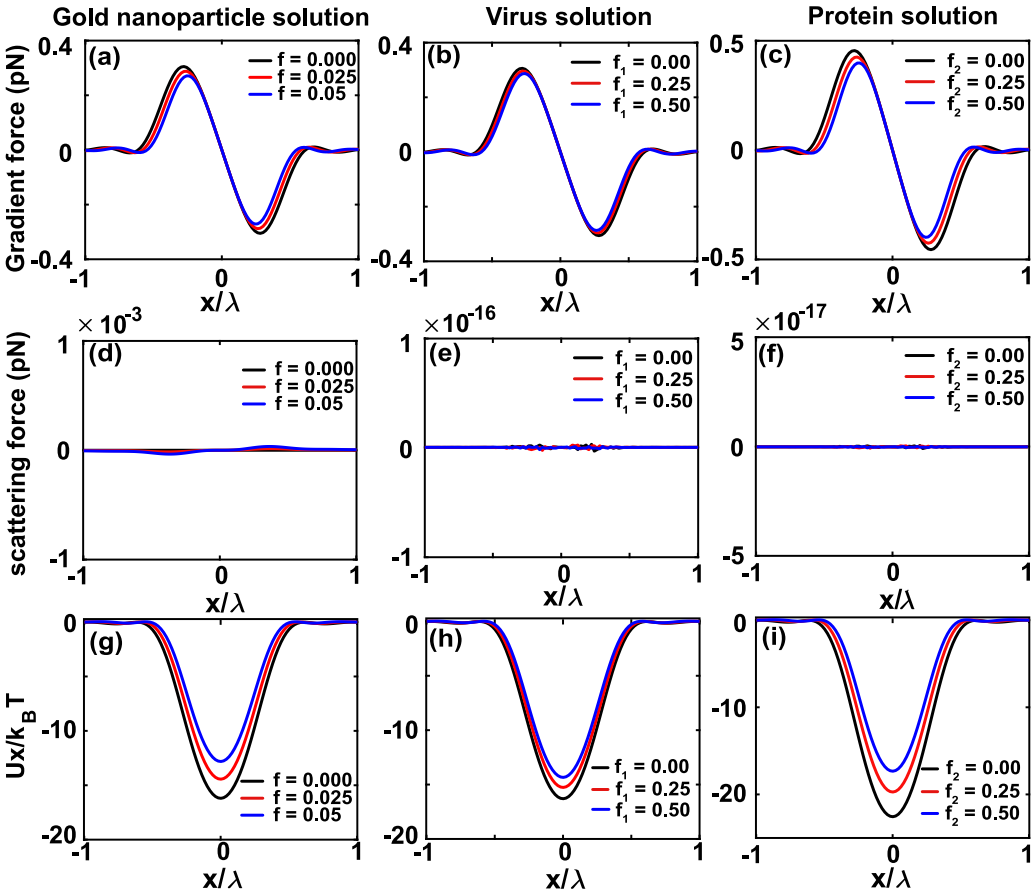

Fig. 3. Distribution of optical forces and potentials on a gold particle with 15 nm radius along x-axis. (a) the gradient force in the gold nanoparticle solution, (d) the scattering force and (g) the corresponding optical potential. The black, red, and blue denote the volume fraction of the gold nanoparticle $f = 0.000$, $f = 0.025$, and $f = 0.05$, respectively. (b), (e) and (h) plot the gradient force, the scattering force and the potential in the virus solution. The black, red, and blue color denote the volume fraction $f_1 = 0$, $f_1 = 0.25$ and $f_1 = 0.5$. For the protein solution, the optical force and potentials are illustrated in (c), (f) and (i). Its volume fraction f_2 is set to 0, 0.25, and 0.5, respectively.

An objective with high NA (NA = 1.2) is selected to focus the incident light. θ_{max} is determined by the NA of the objective lens and the real part of the refractive index of the composite material as $\theta_{max} = \arcsin(\mathrm{NA}/\mathrm{Re}\{\mathbf{n}_{\mathrm{eff}}\})$. According to the vector diffraction theory, the components of the focused electric field and the magnetic field are in terms of cylindrical coordinates $(\rho(\rho = \sqrt{x^2 + y^2}), \varphi, z)$ with origin at the focal point, given by [19]:

$$\mathbf{E} = E_{00}\begin{bmatrix} I_{00} + I_{02}\cos(2\varphi) \\ I_{02}\sin(2\varphi) \\ -2iI_{01}\cos(\varphi) \end{bmatrix}, \tag{11}$$

$$\mathbf{H} = \frac{E_{00}}{Z_{\mu\varepsilon}}\begin{bmatrix} I_{02}\sin(2\varphi) \\ I_{00} - I_{02}\cos(2\varphi) \\ -2iI_{01}\sin(\varphi) \end{bmatrix}, \tag{12}$$

where,

$$I_{00} = \int_0^{\theta_{max}} l(\theta)\sin\theta(1+\cos\theta) \times J_0(k\rho\sin\theta)\exp(ikz\cos\theta)d\theta, \tag{13}$$

$$I_{01} = \int_0^{\theta_{max}} l(\theta)\sin^2\theta \times J_1(k\rho\sin\theta)\exp(ikz\cos\theta)d\theta, \tag{14}$$

$$I_{02} = \int_0^{\theta_{max}} l(\theta)\sin\theta(1-\cos\theta) \times J_2(k\rho\sin\theta)\exp(ikz\cos\theta)d\theta, \tag{15}$$

with,

$$l(\theta) = \frac{ikF}{2\pi}\exp(-ikF)\left(\mathbf{n}_{\mathrm{eff}}\cos\theta\right)^{\frac{1}{2}} \times \exp\left(\frac{-\sin^2\theta}{f_w^2\sin^2\theta_{max}}\right), \tag{16}$$

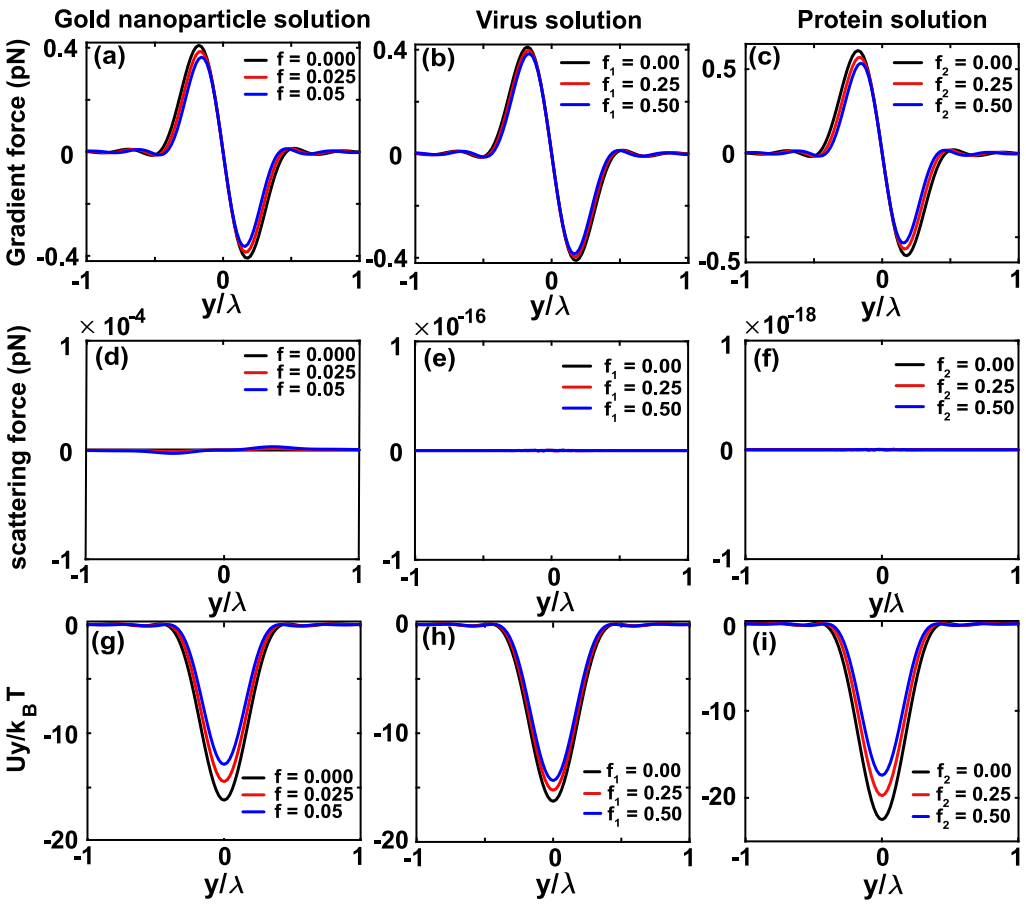

Fig. 4. The optical force and the potential along the y-axis for a gold nanoparticle with a radius of 15 nm. (a), (b) and (c) show the gradient force for different values of the volume fraction along the y-axis in gold nanoparticle solution, virus solution and protein solution, respectively. (d), (e), and (f) plot the scattering force. The corresponding potential along the y-axis in three composite materials is shown in (g), (h), and (i).

where F is the focal distance in the composite material. $Z_{\mu\varepsilon}$ is the wave impedance of the medium where $Z_{\mu\varepsilon} = \sqrt{(\mu_0\mu)/(\varepsilon_0\epsilon_{\text{eff}})}$. J_n is nth-order of the Bessel function of the first kind. The amplitude of the incident light $|E_{00}|^2 = 4P/(\pi w^2 \varepsilon_0 c)$ and the beam radius of incident light is w. We set the filling factor of the objective lens $f_w = 1$ and fix the average power of the incident light at 500 mW in the simulation.

3. Results and discussion

The effective refractive index (n_{eff}) of the composite material with a volume fraction from low to high is calculated using Eqs. (7)–(9). Fig. 2 plots the real and imaginary parts of the refractive index of three composite materials colored blue and red, respectively. In practice, the gold nanoparticle solution is highly dilute in the optical trapping experiment. Therefore, the volume fraction of the gold nanoparticle f is set from 0 to 0.05 in our simulation, as shown in Fig. 2(a). Both the volume fraction of the virus solution f_1 and the protein solution f_2 are set from 0 to 0.5, as shown in Fig. 2.(b) and (c). All of the refractive indices increase at the same time as the volume fraction increases. As the volume fraction gradually increases, changes in the optical properties of the composite material will exert an influence on the optical trapping. For comprehensive analysis, the figure below shows optical forces on gold nanoparticles along three orthogonal directions in three different solutions.

Fig. 3 shows the distribution of optical forces along the x-axis on the gold sphere with a radius of 15 nm in three different solutions. The first solution investigated is the gold nanoparticle solution itself with an incident wavelength of 633 nm. Fig. 3(a), (d), and (g) show the gradient force, scattering force, and potential, respectively, along the x-axis with volume fractions of $f = 0.000$, $f = 0.025$, and $f = 0.05$ (black, red, and blue colors, respectively). In Fig. 3(a), gradient forces are shown as an odd function of x for different values of the volume fraction, while the scattering forces are negligible on the focal plane, as shown in Fig. 3(d). Fig. 3(g) shows the potential with four volume fractions along the x-axis. Although all the depth of the potential well exceed 10 k_BT, the decrease in the depth of the potential well show the reduction of the stability of optical trapping as the increase in volume fraction. Next, the optical trapping in the virus solution is investigated based on the very dilute gold nanoparticle solution ($f = 0.000$), as shown in Fig. 3(b), (e), and (h) with volume fractions of $f_1 = 0$, $f_1 = 0.25$, and $f_1 = 0.5$ (black, red, and blue colors, respectively). The calculation results show that the optical forces and potentials of a gold nanoparticle in the virus solution decrease along the x-axis as the volume fraction increases. Finally, the optical forces and depth of the potential wells in the protein solution are studied based on the optical trapping of a gold nanoparticle with an incident wavelength of 589 nm in Fig. 3(c), (f), and (i) with volume fractions of $f_2 = 0$, $f_2 = 0.25$, and $f_2 = 0.5$ (black, red, and blue colors, respectively).

The optical forces along the y-axis are shown in Fig. 4(a)–(f). The gradient forces on a gold nanoparticle in the gold nanoparticle solution, virus solution, and protein solution are plotted with different volume fractions, as shown in Fig. 4(a), (b), and (c). In the virus solution and the protein solution, the black, red, and blue color indicate the volume fraction f = 0, f = 0.25, and f = 0.5, respectively. Scattering forces in three composite materials are plotted in (d), (e), and (f). The potential along the y-axis is shown in Fig. 4(g), (h), and (i). All optical forces and potentials decrease along the y-axis with increasing volume fraction. Fig. 3 and Fig. 4 demonstrate that the focal point $(0, 0)$ is a position for the stable trapping of a gold nanoparticle in the transverse plane.

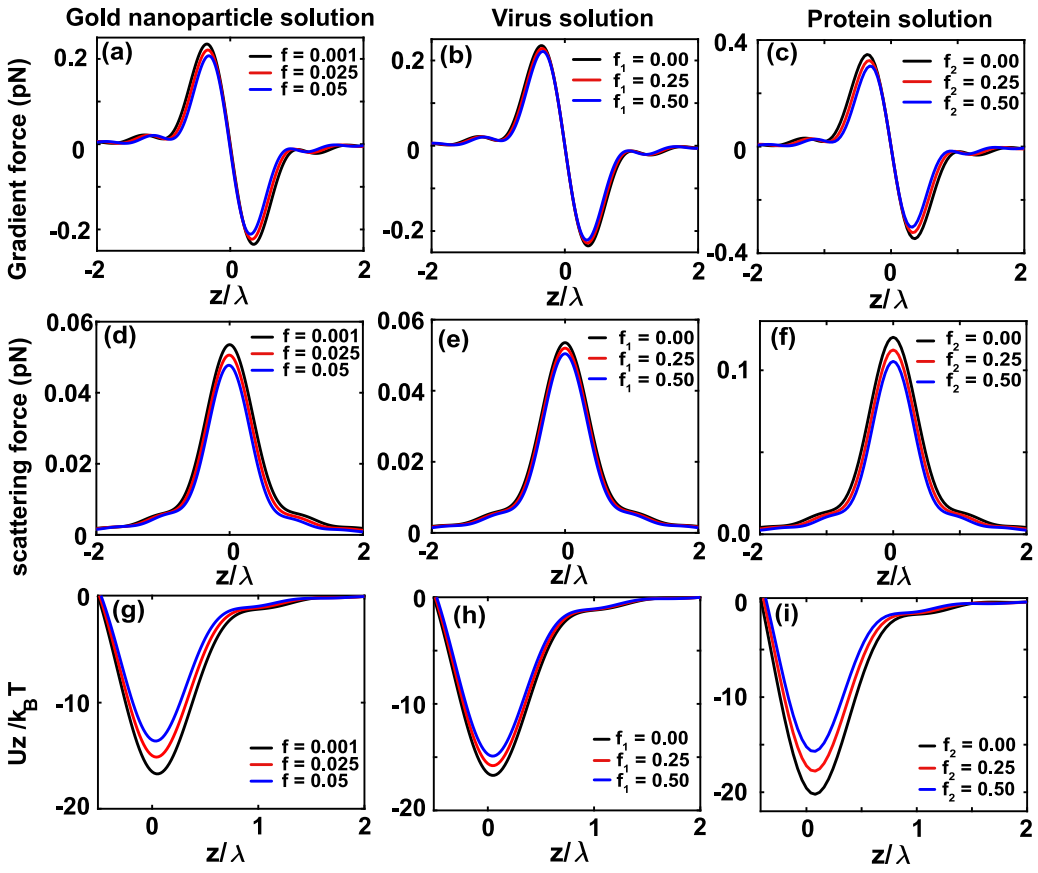

Fig. 5. Distribution of gradient, scattering forces and potentials along the z-axis in three composite materials. (a)–(c) Gradient forces in gold nanoparticle solution, virus solution, and protein solution. (d)–(f) Scattering forces in three solutions. (g)–(i) Optical potentials along z-axis in three solutions.

In the longitudinal plane, $\langle \mathbf{F} \rangle_{\text{grad}}$ and $\langle \mathbf{F} \rangle_{\text{scatter}}$ are calculated along the optical axis (z- axis). In Fig. 5(a)–(c), the magnitude of the gradient force decreases as the volume fraction increases from low to high. Similarly, the scattering force also decreases when the volume fraction increases but always points toward the positive direction of the z-axis, as shown in (d), (e) and (f). $\langle \mathbf{F} \rangle_{\text{total}}$ is the sum of the gradient force and scattering force. The optical potential well is obtained by the Eq. (6) with volume fractions along z-axis, as can be seen in Fig. 5(g), (h), and (i). It has been demonstrated that enhancement and reduction of the transverse trapping stiffness depend on whether the equilibrium position in the focusing or defocusing of the optical field [38,39]. The equilibrium position of the optical trapping is slightly away from the focal plane, as shown in Fig. 5(g), (h) and (i). Therefore, the impact of this displacement of the particle away from the focal point on the trapping stiffness is negligible. According to the calculation results in Figs. 3–5, stable optical trapping can be achieved in three dimensions because all the depth of potential well can exceed 10 $k_B T$ along the x-, y-, and z-axis. Additionally, the results indicate that the volume fraction of the sample is a critical factor affecting the stability of optical trapping in the composite medium. When the volume fraction is increased, the gradient force and potential depth are reduced, leading to a decrease in the stability of optical trapping. Therefore, it is important to consider the volume fraction of the sample when optimizing the conditions for optical trapping.

4. Conclusion

In summary, for the first time to our knowledge, the effect of volume fraction on optical force and potential is analytically investigated based on dipole approximated optical force theory. The correlation between the effective refractive index of the composite material and the volume fractions from low to high is presented for the gold nanoparticle solution, the HIV-1 solution, and the human serum albumin solution. The time-averaged force is calculated on a gold particle with a radius of 15 nm along three orthogonal directions at three different volume fractions. The optical potential is studied in a comparative manner for a given incident power. The stability of the optical trapping is strong enough to allow a gold particle to remain trapped in three composite materials for a long time. According to the calculation results, the greater the volume fraction, the shallower the potential well depth. Thus, at a high volume fraction, it is more difficult to achieve stable optical trapping in the sample solution. The model can therefore be used to provide theoretical support for achieving more efficient optical trapping of gold nanoparticles in a wide range of applications.

Declaration of competing interest

The authors declare that they have no known competing financial interests or personal relationships that could have appeared to influence the work reported in this paper.

Data availability

Data will be made available on request.

Acknowledgments

Guangdong Major Project of Basic and Applied Basic Research (2020B0301030009); National Natural Science Foundation of China (62175157, U1701661, 61935013, 61975128); Leading Talents of Guangdong Province Program (00201505); Natural Science Foundation of Guangdong Province, China (2019TQ05X750); Science and Technology Innovation Commission of Shenzhen (JCYJ20180507182035270,

KQTD20170330110444030, ZDSYS201703031605029); Shenzhen Fundamental Research Fund (JCYJ20180305125209538).

References

[1] A. Ashkin, Acceleration and trapping of particles by radiation pressure, Phys. Rev. Lett. 24 (1970) 156–159, http://dx.doi.org/10.1103/PhysRevLett.24.156.

[2] C. Keir, Neuman, Attila, Nagy, Single-molecule force spectroscopy: optical tweezers, magnetic tweezers and atomic force microscopy., Nature Methods (2008) http://dx.doi.org/10.1038/nmeth.1218.

[3] Y. Yu, T.-H. Xiao, Y. Wu, W. Li, Q.-G. Zeng, L. Long, Z.-Y. Li, Roadmap for single-molecule surface-enhanced Raman spectroscopy, Adv. Photonics 2 (11) (2020) 014002, http://dx.doi.org/10.1117/1.AP.2.1.014002.

[4] E.J. Bjerneld, F. Svedberg, M. Käll, Laser-induced growth and deposition of noble-metal nanoparticles for surface-enhanced Raman scattering, Nano Lett. 3 (5) (2003) 593–596, http://dx.doi.org/10.1021/nl034034r.

[5] Huang, Honglian, Guo, Jiafang, Li, Lin, Ling, Baohua, Feng, Zhi-Yuan, Optical trapping of gold nanoparticles by cylindrical vector beam, Opt. Lett. 37 (10) (2012) 1694–1696, http://dx.doi.org/10.1364/OL.37.001694.

[6] K. Svoboda, S.M. Block, Optical trapping of metallic Rayleigh particles, Opt. Lett. 19 (13) (1994) 930–932, http://dx.doi.org/10.1364/OL.19.000930.

[7] X. Huang, P.K. Jain, I.H. El-Sayed, M.A. El-Sayed, Gold nanoparticles: interesting optical properties and recent applications in cancer diagnostics and therapy, Nanomedicine 2 (5) (2007) 681–693, http://dx.doi.org/10.2217/17435889.2.5.681.

[8] S.-J. Park, T.A. Taton, C.A. Mirkin, Array-based electrical detection of DNA with nanoparticle probes, Science 295 (5559) (2002) 1503–1506, http://dx.doi.org/10.1126/science.1067003.

[9] J.S. Lee, P.A. Ulmann, M.S. Han, C.A. Mirkin, A DNA-gold nanoparticle-based colorimetric competition assay for the detection of cysteine, Nano Lett. 8 (2) (2008) 529, http://dx.doi.org/10.1021/nl0727563.

[10] P. Yupapin, Aziz, N. Suwanpayak, Ma, Jalil, Saktioto, Ali, Gold nanoparticle trapping and delivery for therapeutic applications, Int. J. Nanomedicine 7 (default) (2012) 11–17, http://dx.doi.org/10.3389/fbioe.2021.647905.

[11] N. Wangoo, C.R. Suri, G. Shekhawat, Interaction of gold nanoparticles with protein: A spectroscopic study to monitor protein conformational changes, Appl. Phys. Lett. 92 (13) (2008) 1323, http://dx.doi.org/10.1063/1.2902302.

[12] F. Hajizadeh, S.S. Reihani, Optimized optical trapping of gold nanoparticles, Opt. Express 18 (2) (2010) 551–559, http://dx.doi.org/10.1364/OE.18.000551.

[13] Y. Qin, L.-M. Zhou, L. Huang, Y. Jin, H. Shi, S. Shi, H. Guo, L. Xiao, Y. Yang, C.-W. Qiu, et al., Nonlinearity-induced nanoparticle circumgyration at sub-diffraction scale, Nature Commun. 12 (1) (2021) 1–8, http://dx.doi.org/10.1038/s41467-021-24100-0.

[14] L.-M. Zhou, Y. Shi, X. Zhu, G. Hu, G. Cao, J. Hu, C.-W. Qiu, Recent progress on optical micro/nanomanipulations: Structured forces, structured particles, and synergetic applications, ACS Nano 16 (9) (2022) 13264–13278, http://dx.doi.org/10.1021/acsnano.2c05634.

[15] O.M. Maragò, P.H. Jones, P.G. Gucciardi, G. Volpe, A.C. Ferrari, Optical trapping and manipulation of nanostructures, Nature Nanotechnol. 8 (11) (2013) 807–819, http://dx.doi.org/10.1038/nnano.2013.208.

[16] P.M. Hansen, V.K. Bhatia, N. Harrit, L. Oddershede, Expanding the optical trapping range of gold nanoparticles, Nano Lett. 5 (10) (2005) 1937–1942, http://dx.doi.org/10.1021/nl051289r.

[17] M. Friebel, M.C. Meinke, Determination of the complex refractive index of highly concentrated hemoglobin solutions using transmittance and reflectance measurements, J. Biomed. Opt. 10 (6) (2005) 064019, http://dx.doi.org/10.1117/1.2138027.

[18] V.V. Tuchin, et al., Tissue Optics, Society of Photo-Optical Instrumentation Engineers (SPIE), Bellingham, WA, USA, 2015, http://dx.doi.org/10.1117/3.1003040.

[19] L. Novotny, B. Hecht, Principles of Nano-Optics, Cambridge University Press, 2012, http://dx.doi.org/10.1017/CBO9780511794193.

[20] S. Albaladejo, M.I. Marqués, M. Laroche, J.J. Sáenz, Scattering forces from the curl of the spin angular momentum of a light field, Phys. Rev. Lett. 102 (2009) http://dx.doi.org/10.1103/PhysRevLett.102.113602.

[21] P. Chaumet, M. Nieto-Vesperinas, Time-averaged total force on a dipolar sphere in an electromagnetic field, Opt. Lett. 25 (15) (2000) 1065–1067, http://dx.doi.org/10.1364/OL.25.001065.

[22] S. Yadav, A. Devi, A.K. De, Synergistic effect of Fano resonance and optical nonlinearity in laser trapping of silver nanoparticles, Phys. Rev. A 102 (2020) 043511, URL https://link.aps.org/doi/10.1103/PhysRevA.102.043511.

[23] A. Devi, S.S. Nair, A.K. De, Disappearance and reappearance of an optical trap for silver nanoparticles under femtosecond pulsed excitation: A theoretical investigation, Europhys. Lett. 126 (2) (2019) 28002, http://dx.doi.org/10.1209/02955075/126/28002.

[24] C.F. Bohren, D.R. Huffman, Absorption and scattering of light by small particles, John Wiley & Sons, Ltd, ISBN: 9783527618156, 1998, pp. 130–157, http://dx.doi.org/10.1002/9783527618156.ch5.

[25] J.D. Jackson, Classical electrodynamics, 3rd ed., Amer. J. Phys. 67 (1999) 841–842, http://dx.doi.org/10.1119/1.19136.

[26] B.T. Draine, The discrete-dipole approximation and its application to interstellar graphite grains, Astrophys. J. 333 (1988) 848, http://dx.doi.org/10.1086/166795.

[27] P. Mallet, C. Guérin, A. Sentenac, Maxwell-garnett mixing rule in the presence of multiple scattering: derivation and accuracy, Phys. Rev. B 72 (1) (2005) 014205, http://dx.doi.org/10.1103/PhysRevB.72.014205.

[28] U. Kreibig, M. Vollmer, Optical Properties of Metal Clusters, Springer, Berlin, 1975, http://dx.doi.org/10.1016/B978-0-323-90879-5.00010-X.

[29] C. Min, Z. Shen, J. Shen, Y. Zhang, H. Fang, G. Yuan, L. Du, S. Zhu, T. Lei, X. Yuan, Focused plasmonic trapping of metallic particles, Nature Commun. 4 (1) (2013) 1–7, http://dx.doi.org/10.1038/ncomms3891.

[30] A. Devi, A.K. De, Theoretical investigation on nonlinear optical effects in laser trapping of dielectric nanoparticles with ultrafast pulsed excitation, Opt. Express 24 (19) (2016) 21485–21496, http://dx.doi.org/10.1364/OE.24.021485.

[31] Anays, Acevedo-Barrera, Augusto, Garcia-Valenzuela, Analytical approximation to the complex refractive index of nanofluids with extended applicability, Opt. Express 27 (20) (2019) 28048–28061, http://dx.doi.org/10.1364/OE.27.028048.

[32] O. Block, A. Mitra, L. Novotny, C. Dykes, A rapid label-free method for quantitation of human immunodeficiency virus type-1 particles by nanospectroscopy, J. Virol. Methods 182 (1–2) (2012) 70–75, http://dx.doi.org/10.1016/j.jviromet.2012.03.012.

[33] V. Twersky, Absorption and multiple scattering by biological suspensions, JOSA 60 (8) (1970) 1084–1093, http://dx.doi.org/10.1364/JOSA.60.001084.

[34] T. Vo-Dinh, Biomedical Photonics Handbook: Biomedical Diagnostics, CRC Press, 2014, http://dx.doi.org/10.1201/9780203008997.

[35] T.L. McMeekin, M.L. Groves, N.J. Hipp, Refractive indices of amino acids, proteins, and related substances, ACS Publications, 1964, pp. 54–66, http://dx.doi.org/10.1021/ba-1964-0044.ch004.

[36] M. Kiselev, G. IuA, G. Dobretsov, M. Komarova, Size of a human serum albumin molecule in solution, Biofizika 46 (3) (2001) 423–427, URL https://pubmed.ncbi.nlm.nih.gov/11449540/.

[37] P. Johnson, R. Christy, Optical constants of the noble metals, Phys. Rev. B 6 (12) (1972) 4370–4379, http://dx.doi.org/10.1103/PhysRevB.6.4370.

[38] A. Ivinskaya, M.I. Petrov, A.A. Bogdanov, I. Shishkin, P. Ginzburg, A.S. Shalin, Plasmon-assisted optical trapping and anti-trapping, Light Sci. Appl. 6 (5) (2017) e16258, http://dx.doi.org/10.1038/lsa.2016.258.

[39] G.C. Messina, X. Zambrana-Puyalto, N. Maccaferri, D. Garoli, F. De Angelis, Two-state switchable plasmonic tweezers for dynamic manipulation of nano-objects, Nanoscale 12 (15) (2020) 8574–8581, http://dx.doi.org/10.1039/D0NR00721H.